J. Membrane Biol. 197, 155–168 (2004)
DOI: 10.1007/s00232-004-0650-6

The Journal of
Membrane
Biology

Channel Activation Voltage Alone Is Directly Altered in an Isoform-specific Manner by $Na_{v1.4}$ and $Na_{v1.5}$ Cytoplasmic Linkers

E.S. Bennett
Department of Physiology & Biophysics and Program in Neuroscience, University of South Florida College of Medicine, Tampa, FL 33612, USA

Received: 8 July 2003/Revised: 29 November 2003

Abstract. The isoform-specific direct role of cytoplasmic loops in the gating of two voltage-gated sodium channel isoforms, the human cardiac channel ($Na_{v1.5}$; hH1) and the human adult skeletal muscle channel ($Na_{v1.4}$; hSkM1), was investigated. Comparison of biophysical characteristics was made among hSkM1, hH1, and several hSkM1/hH1 chimeras in which the putative cytoplasmic loops that join domain I to II (loop A) and domain II to III (loop B) from one isoform replaced one or both of the analogous loops from the other isoform. For all parameters measured, hSkM1 and hH1 behavior were significantly different. Comparison of hSkM1 and hH1 biophysical characteristics with the function of their respective chimeras indicate that only the half-activation voltage (V_a) is directly and differently altered by the species of cytoplasmic loop such that a channel consisting of one or both hSkM1 loops activates at smaller depolarizations, while a larger depolarization is required for activation of a channel containing one or both of the analogous hH1 loops. When either cardiac channel loop A or B is attached to hSkM1, a 6–7 mV depolarizing shift in V_a is measured, increasing to a nearly 20 mV depolarization when both cardiac-channel loops are attached. The addition of either skeletal muscle-channel loop to hH1 causes a 7 mV hyperpolarization in V_a, which increases to about 10 mV for the double loop chimera. There is no significant difference in either steady-state inactivation or in the recovery from inactivation data between hSkM1 and its chimeras and between hH1 and its chimeras. Data indicate that the cytoplasmic loops contribute directly to the magnitude of the window current, suggesting that channels containing skeletal muscle loops have three times the peak persistent channel activity compared to channels containing the cardiac loops. An electrostatic mechanism, in which surface charge differences among these loops might alter differently the voltage sensed by the gating mechanism of the channel, can not account for the observed isoform-specific effects of these loops only on channel activation voltage. In summary, although the DI-DII and DII-DIII loop structures among isoforms are not well conserved, these data indicate that only one gating parameter, V_a is affected directly and in an isoform-specific manner by these divergent loop structures, creating loop-specific window currents and percentages of persistently active channels at physiological voltages that will likely impact the excitability of the cell.

Key words: Voltage-gated sodium channels — Ion channels — Ion channel gating — Window current — Cardiac — Skeletal muscle

Introduction

Voltage-gated sodium channels are responsible for the initiation and propagation of nerve, skeletal muscle, and cardiac action potentials. The orchestrated activation and inactivation gating of sodium channels is vital to normal neuronal signaling, skeletal muscle contraction, and normal heart rhythms. Even small syncopations from this normal gating rhythm may alter cellular excitability and whole-animal physiology significantly. Several genetic sodium channel diseases have been described, with multiple mutations leading to similar disease phenotypes. Diseases such as paramyotonia congenita (PMC), hyperkalemic periodic paralysis (HYPP), and long QT syndrome (LQTS), are all examples of well-studied genetic ion channel diseases of skeletal muscle and cardiac voltage-gated sodium channels

Correspondence to: E.S. Bennett; email: esbennet@hsc.usf.edu

(*see*, e.g., Cannon, Brown Jr. & Corey, 1991; Ptacek et al., 1991, 1992; Cummins et al., 1993; Chahine et al., 1994; Bennett et al., 1995; Dumaine et al., 1996; Fan et al., 1996; Hayward, Brown Jr. & Cannon, 1996; Ji et al., 1996; Lawrence et al., 1996; Lerche et al., 1996; Wang et al., 1996; Nagatomo et al., 1998; Wei et al., 1999; Schwartz et al., 2000; Abriel et al., 2001; Splawski et al., 2002). These mutant channels typically show small "persistent" sodium currents when studied in vitro, caused primarily by a tiny percentage of mutant channels residing in the active state longer than the wild-type channel. There are several possible molecular mechanisms that could lead to this persistent current, one of which is a change in the magnitude and/or voltage-range of the so-called "window current" (see, e.g., Wang et al., 1996; Abriel et al., 2001; Splawski et al., 2002). The window current is the intersecting area under the overlapping conductance-voltage and steady-state inactivation curves, and it represents the voltage range at which a small percentage of channels is persistently active. Such activity would lead to a small, persistent inward current and slight depolarization of the membrane, consistent with that observed in LQTS, HYPP, and PMC. In addition to muscle sodium channelopathies, recent work on naturally occurring mutations of SCN1A ($Na_{v1.1}$), which appear to be responsible for inherited epilepsy, show similar effects on channel function. That is, an increase in the window current may be responsible for the creation of a hyperexcitable mutant SCN1A that leads to seizures (Lossin et al., 2002; Spampanato et al., 2003). In all of these examples, channel function is only minimally affected, with a tiny increase in persistent channel activity on the order of 1%, yet the whole-animal phenotype is altered significantly. Patients present with such symptoms as muscle paralysis, myotonia, cardiac arrhythmias, or seizures caused by the slight redistribution of channels from one functional state to another and/or a slight change in resting membrane potential.

Recent studies from our lab revealed a novel functional difference between two sodium channel isoforms, the adult skeletal muscle sodium channel ($Na_{v1.4}$) and the cardiac sodium channel ($Na_{v1.5}$). The studies described apparent differences in the activation mechanisms between the two isoforms. We showed in Bennett, 1999, that while internal papain treatment removed both $Na_{v1.4}$ and $Na_{v1.5}$ fast inactivation, the half-activation voltage (V_a) for $Na_{v1.5}$ was shifted dramatically in the hyperpolarized direction with no significant impact on V_a for $Na_{v1.4}$. The effect of papain on $Na_{v1.5}$ V_a was shown to be direct and not a result of the uncoupling of inactivation from activation. Together, the data implied that cytoplasmic structural differences between cardiac and skeletal muscle sodium channel isoforms exist that differently impact channel activation.

The second report set out to determine specific cytoplasmic regions of the cardiac sodium channel responsible for this papain-induced shift in V_a (Bennett, 2001). Functional comparison of $Na_{v1.4}/Na_{v1.5}$ chimeras indicated that the first two cytoplasmic loops (loops A and B, respectively) of the cardiac sodium channel joining domain I to II and domain II to III are both necessary and together sufficient to produce a significant shift in the voltage at which the cardiac channel activates. This measured shift in V_a was observed even in the absence of papain, albeit in the opposite direction, indicating that these loops, intact, or disrupted following papain treatment, have some effect on the voltage dependence of channel gating.

It is not surprising that one observes isoform-specific functional effects of these cytoplasmic loops, as these loops are among the least conserved channel structures across the voltage-gated sodium channel family. Thus, one might expect significant functional differences imposed by such diverse structures. While the previous studies measured isoform-specific changes in steady-state activation voltage correlated to apparently disrupted cytoplasmic loops following papain treatment, data linking these different loops to direct effects on other specific gating mechanisms was not determined.

As such, there are several possible mechanisms that might produce the measured shifts in channel activation voltage observed following papain treatment: 1) An exclusive, isoform-specific direct effect of these loops on channel activation voltage; 2) the specific loop attached to a channel may impose multiple effects on various gating parameters; 3) a given loop may impose the same or similar effect(s) on all gating parameters; or 4) direct, isoform-specific effects of these loops on gating mechanisms other than activation that are observed as shifts in channel activation voltage due to the kinetic coupling among functional channel states. Any of these four possibilities are plausible. Thus, more direct measurements of various gating parameters are needed in order to determine more conclusively the isoform-specific role of these cytoplasmic loops in channel function.

Here we investigate these possibilities by measuring the differential (or lack thereof) effects of cytoplasmic loop(s) A (DI-DII linker) and/or B (DII-DIII linker) of the human cardiac ($Na_{v1.5;}$ hH1) versus skeletal muscle ($Na_{v1.4}$; hSkM1) sodium channels on several channel gating mechanisms, all in the absence of papain. We measure and compare activation, inactivation, and recovery parameters for hSkM1 and hH1 and six chimeras in which one or both loop(s) A and B of hSkM1 and hH1 are swapped. For all parameters measured, hSkM1 and hH1 behavior are significantly different. However, comparison of the biophysical characteristics of hSkM1 and hH1 with the function of their respective

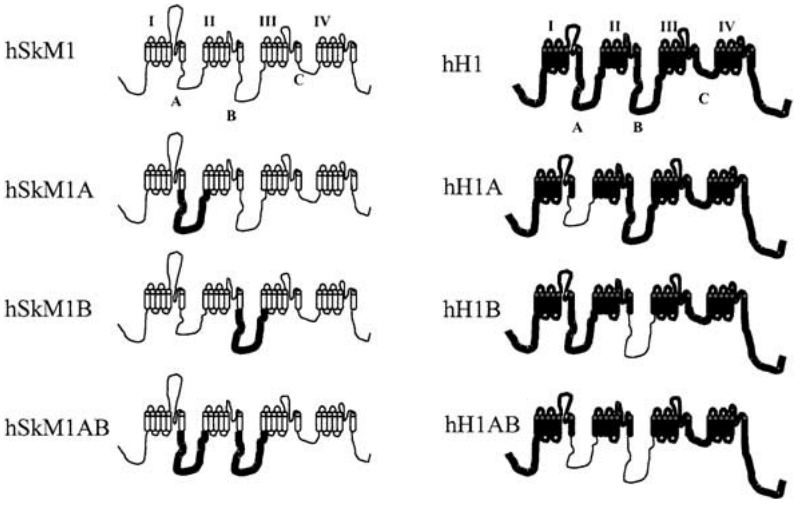

Fig. 1. Schematic depicting hSkM1, hH1, and tested chimeras. Figure depicts the wild-type channels and chimeras studied throughout this report. A schematic of hSkM1 and hH1 head the left and right columns, respectively. The corresponding chimeras are shown below their respective wild-type isoforms. For example, chimeras consisting primarily of hSkM1 and of one or two hH1 cytoplasmic loops are depicted in the hSkM1 column. Nomenclature used is consistent with that used previously (Makita et al., 1996; Bennett, 2001).

single and double loop chimeras indicate that only the half-activation voltage (V_a) is directly and differently affected by the species of cytoplasmic loop such that a channel activates at smaller depolarizations if it contains one or both of the hSkM1 loops, while a larger depolarization is required if the channel contains one or both of the analogous hH1 loops. Neither steady-state inactivation nor the recovery from inactivation is altered by swapping loops. The window current, however, shows a marked dependence on the species of loop attached to the channel, such that peak persistent channel activity in the presence of the skeletal muscle channel loops is predicted to be more than three times the peak persistent activity of channels containing the cardiac channel loops. Together, these data indicate that although these two cytoplasmic loops of hH1 and hSkM1 are structurally divergent, only one gating parameter, channel activation voltage, is directly and differently affected, creating a change in the level of persistent activation that will likely impact the excitability of the cell. Initial studies of the mechanism responsible for this phenomenon indicate that any internal surface charge differences among these loops that might alter differently the voltage sensed by the gating mechanism of the channel (i.e., an electrostatic mechanism) can not account for the observed isoform-specific effects of these loops only on channel activation voltage.

Materials and Methods

CHO Cell-Transfection and Tissue Culture Methods

All constructs used were either created or subcloned as described in Bennett, 2001, and are shown schematically in Fig. 1. CHO cells were transfected with each vector using lipofectamine technology as previously described (Bennett, 1999). Briefly, CHO cells were passaged onto 35 mm culture plates at about 25% confluence. Following a 24 hour incubation, cells were then exposed to a 1 ml Opti-MEM (GIBCO Life Technologies) medium containing 8 μl lipofectamine (GIBCO) and 1–2 μg DNA, consisting of about 12% pGreen Lantern-1 (GFP; GIBCO), and about 88% sodium channel expression vector. Following a 5–24 hour incubation at 37°C in a 5% CO_2 humidified incubator, the medium was exchanged for normal, non-selective CHO cell-growing medium. A post-transfection incubation of 68–76 hours preceded the electrophysiological recordings, selecting cells expressing GFP. As described previously, GFP had no effect on sodium channel function (Bennett, 1999).

Whole-Cell Recording of Sodium Currents in CHO Cells

Transfected cells were studied using the patch-clamp whole-cell recording technique described previously (Bennett et al, 1997). An Axon Instruments 200B patch-clamp amplifier with a CV203BU headstage (Axon Instruments) was used in combination with a Nikon TE300 inverted microscope. Pulse protocols were generated using a 200 MHz Pentium II or 800 MHz Pentium III PC computer (Dell Computers) running Pulse acquisition software (HEKA). The resultant analog signals were filtered at 5 kHz using an eight-pole Bessel filter (Frequency Devices - 9200 LPF) and then digitized using the ITC-16 AD/DA converter (Instrutech).

The Sutter micromanipulator, MP-285, was used to place the electrode onto the cell. Electrode glass (Drummond capillary tubes, 2-000-210) was pulled using a two-step process on a Sutter (model P-87) electrode puller to a resistance of 1–2 MΩ measured in the salt solutions used. The external solution used was (in mM): 224 sucrose, 22.5 NaCl, 4 KCl, 2.0 $CaCl_2$, 5 glucose, and 5 HEPES, while the internal solution used was (in mM): 120 sucrose, 60 CsF, 32.5 NaCl, and 5 HEPES (titrated with 1N NaOH to pH = 7.4 at room temperature). Although series resistance was compensated 95–98% for all data, the smaller current produced using the low-sodium solutions further minimized any remaining series resistance error, resulting in < 1mV error. The phenomena reported here were unaffected by the use of these solutions, as indicated by the fact that the half-activation voltages measured for the two wild-type channels (hSkM1 and hH1) and the two double-loop chimeras (hSkM1AB and hH1AB) under more physiological Na^+ gradients (132 mM Na^+ extracellular, 11.5 mM Na^+ intracellular) were not significantly different from those indicated in Table 1 measured under the outward Na^+ gradients used in this study. All data

Table 1. Gating parameters for hSkM1, hH1 and the single- and double-loop chimeras

Na^+ channel construct	n	V_a (mV)	K_a (mV)	V_i (mV)	K_i (mV)	τ_h (−20 mV) (ms)	τ_{rec}(−120 mV) (ms)
hSKM1	9	−25.9 ± 1.9	−7.0 ± 0.5	−56.0 ± 1.1	5.4 ± 0.3	1.1 ± 0.1	0.92 ± 0.04
hSkM1A	9	−19.1* ± 2.3	−7.3 ± 0.8	−55.5 ± 2.3	5.7 ± 0.5	1.3 ± 0.1	
hSkM1B	9	−19.6* ± 1.9	−7.8 ± 0.3	−58.2 ± 1.8	5.1 ± 0.2	1.6 ± 0.3	
hSkM1AB	9	−6.5*** ± 2.2	−7.6 ± 0.5	−53.0 ± 2.4	6.0 ± 0.5	3.3** ± 0.8	0.92 ± 0.03
hH1	13	−20.2 ± 1.5	−8.3 ± 0.6	−64.9 ± 2.7	7.1 ± 0.9	2.2 ± 0.2	2.9 ± 0.1
hH1A	8	−26.0* ± 3.0	−9.1 ± 0.6	−69.1 ± 4.0	6.6 ± 0.5	1.4*** ± 0.1	
hH1B	9	−25.3* ± 2.8	−9.3 ± 0.6	−68.2 ± 2.8	6.5 ± 0.2	1.4*** ± 0.1	
hH1AB	7	−28.8** ± 2.8	−8.3 ± 0.6	−66.9 ± 3.4	7.1 ± 0.5	1.3*** ± 0.1	3.1 ± 0.1

Data list the mean parameter value ± SEM for six gating parameters measured for hSkM1, hH1, single- and double-loop chimeras. Significance was tested throughout by comparing chimera function with wild-type channel function using a two-tailed test, demarcating significance as follows: *significant ($p < 0.05$); **very significant ($p < 0.01$); ***highly significant, ($p < 0.005$).

shown are recorded at least 5 minutes after attaining whole cell configuration to assure complete dialysis of the intracellular solution. All experiments were performed at room temperature (22–24°C). All solutions were filtered using Gelman 0.2 μm filters immediately prior to use.

Pulse Protocols

Conductance-Voltage (G-V) Relationship

The cell was held at −100 mV, stepped to various depolarized potentials (ranging from −100 to +70 mV in 10 mV increments) for 10 ms, and then returned to the holding potential. Consecutive pulses were stepped every 1.5 seconds and the data were leak-subtracted using the P/4 method, stepping negatively from the −100 mV holding potential. At each test potential, steady-state whole-cell conductance was determined by measuring the peak current at that potential and dividing by the driving force (i.e., difference between the membrane potential and the observed reversal potential). The maximum conductance generated by each cell was used to normalize the data for each cell to its maximum conductance by fitting the data to a single Boltzmann distribution (equation 1, solving for maximum conductance). The average V_a +/− SEM and K_a +/− SEM values listed in Table 1 are determined from these single Boltzmann distributions. The normalized data were then averaged with those from other cells, and the resultant average conductance-voltage curve was fit via least squares using the following Boltzmann relation:

$$\text{Fraction of maximal conductance} = [1 + \exp -(V - V_a/K_a)]^{-1}, \quad (1)$$

where V is the membrane potential, V_a is the voltage of half-activation, and K_a is the slope factor.

Measurement of Inactivation Time Constants

Inactivation time constants were determined by fitting the current traces used to measure G-V relationships. Attenuating currents from 90 to 10% of the peak values were fit to a single-exponential function to determine the time course of fast inactivation.

Steady-State Inactivation Curves (h_{inf})

Voltage dependence of steady-state inactivation was determined by first prepulsing the membrane for 500 ms from the −100 mV holding potential, then stepping to +60 mV for 5 ms, and then returning to the −100 mV holding potential. The prepulse voltages ranged from −130 mV to +10 mV in 10 mV increments. The currents from each cell were normalized to the maximum current measured by fitting each single cell data to a single Boltzmann distribution (equation 2, solving for maximum current), from which the mean V_i ± SEM and K_i ± SEM values listed in Table 1 were determined. The normalized data for many cells were then averaged and fit to Eq. 2, from which the mean V_i and K_i describing steady-state inactivation for the channel population were calculated.

$$\text{Fraction of maximum current} = [1 + \exp((V - V_i)/K_i)]^{-1} \quad (2)$$

Recovery from Inactivation

Cells were held at −100 mV, then stepped to +60 mV for 10 ms and returned to the recovery potential for varying duration ranging from 1 to 20 ms in 1 ms increments. Following this recovery pulse, the potential was again stepped to +60 mV for 10 ms. The peak current measured during the two +60 mV depolarizations were compared, and the fractional peak current remaining during the second depolarization was plotted as a function of the recovery pulse duration. This represents the fraction of channels that recovered from inactivation during the recovery interval. Time constants of recovery were determined by fitting the data to single-exponential functions.

Data analysis

The data were analyzed using a combination of Pulse/PulseFit (HEKA) and SigmaPlot 2001 (SSPS Inc.) software.

Results

Activation Voltages Are Directly and Consistently Dependent on the Species of Cytoplasmic Loop(s) Attached to the Channel

Our previous studies showed that intracellular papain treatment caused a shift in the voltage dependence of cardiac sodium-channel activation (Bennett, 1999).

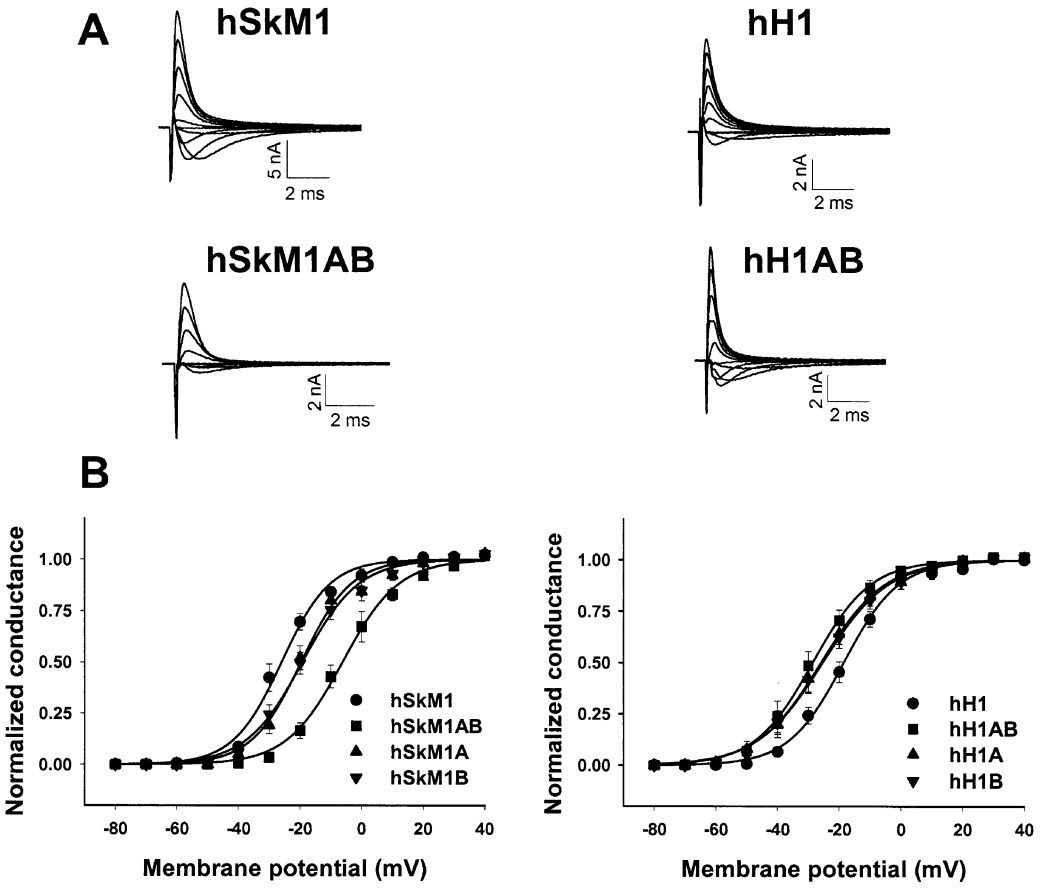

Fig. 2. Channel activation voltage is more depolarized for channels containing hH1 loops A and/or B than for channels containing the analogous hSkM1 loops. *Panel A*: Whole-cell current traces from CHO cells transfected with hSkM1, hH1, hSkM1AB, and hH1AB. Currents recorded during 10 ms test pulses ranging from −50 to +60 mV in 10 mV increments, stepped from the −100 mV resting potential. *Panel B*: Conductance-voltage (*G-V*) relationships for all tested constructs. Data are the average normalized peak conductance ± SEM at a membrane potential. Curves are fits of the data to single Boltzmann distributions. *Left panel*: *G-V* for hSkM1, hSkM1A, hSkM1B, and hSkM1AB. *Circles*: hSkM1; *triangles*: hSkM1A; *inverted triangles*: hSkM1B; squares: hSkM1AB. $n = 9$ for each set of data. *Right Panel*: *G-V* for hH1, hH1A, hH1B, and hH1AB. *Circles*: hH1 ($n = 13$); *triangles*: hH1A ($n = 8$); *Inverted triangles*: hH1B ($n = 9$); *squares*: hH1AB ($n = 7$).

The cardiac channel structures responsible for this phenomenon were localized to two cytoplasmic loops: the loops joining domain I to II and domain II to III, with each loop contributing nearly equally to the measured shifts in channel activation voltage following their apparent disruption through papain treatment (Bennett, 2001). Here, several biophysical gating parameters of hSkM1 and hH1 and the six chimeras shown in Fig. 1 (four single-loop chimeras and two double-loop chimeras) are characterized in the absence of papain to determine the direct isoform-specific effect(s) of these cytoplasmic loops on channel function. This is done in an effort to glean a mechanism by which these cytoplasmic loops contribute to channel function in an isoform-specific manner.

Figure 2*A* shows examples of whole-cell current traces from cells transfected with the two wild-type channels, $Na_{v1.4}$ (hSkM1) and $Na_{v1.5}$ (hH1), as well as the two double-loop chimeras, hSkM1AB, and hH1AB. All constructs tested produced nanoampere-level Na^+ currents with activation and fast inactivation rates within the normal range. Figure 2*B* compares the conductance voltage (*G-V*) relationships for hSkM1 and its chimeras (*left panel*), and for hH1 and its chimeras (*right panel*). Note that when either cardiac channel loop A or B is attached to hSkM1 (chimeras, hSkM1A and hSkM1B), similar 6–7 mV depolarizing shifts in V_a are measured, with a nearly 20 mV depolarization in V_a observed when both cardiac channel loops are attached (hSkM1AB). The addition of skeletal muscle channel loops to hH1 causes a hyperpolarization in V_a, shifting by about 7 mV for each single-loop chimera and by about 10 mV for the double-loop chimera. Together the data suggest that, for a given isoform, loops A and B each contribute similarly to the effect on channel activation voltage. In addition, the data indicate that for a given construct (i.e., for hSkM1 or for hH1), channels containing one or both of the cardiac channel cyto-

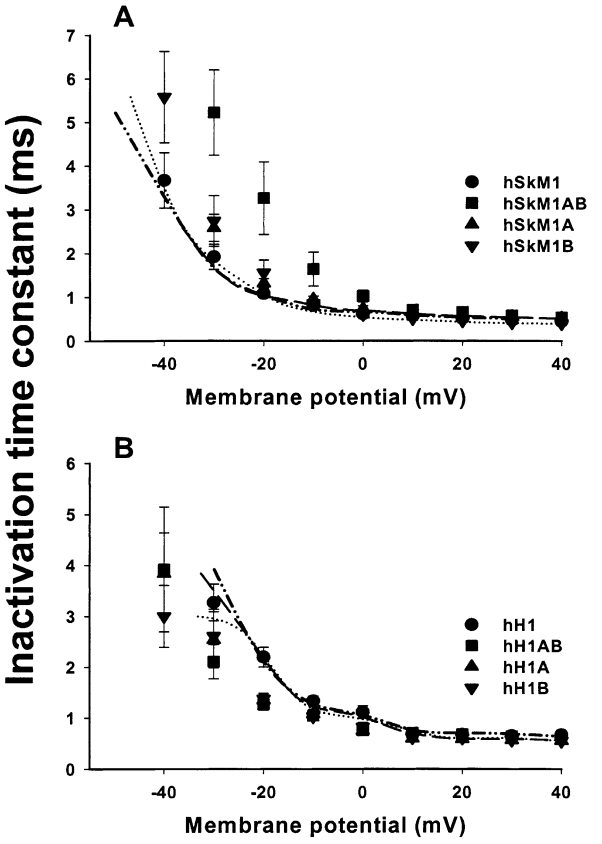

Fig. 3. The effect of a specific cytoplasmic loop(s) on the rate of fast inactivation mimics its effect on channel activation voltage. Time constants of inactivation (τ_h) as a function of membrane potential. Data are the average time constants of inactivation ± SEM. (*A*) τ_h for hSkM1, hSkM1A, hSkM1B, and hSkM1AB. *Circles*: hSkM1; *triangles*: hSkM1A, *inverted triangles*: hSkM1B; *squares*: hSkM1AB. $n = 9$ for each set of data. Lines represent point-to-point curves of the chimera data "shifted" by 6–19 mV in the hyperpolarized direction along the voltage axis. The magnitude of the imposed shift was determined by the shift in V_a measured in Fig. 2. *Long dash*: hSkM1A shifted 6.8 mV. *dots*: hSkM1B shifted 6.3 mV; *dash-dot-dot*: hSkM1AB shifted 19.4 mV. (*B*) τ_h for hH1, hH1A, hH1B, and hH1AB. *Circles*: hH1 ($n = 13$); *triangles*: hH1A ($n = 8$); *inverted triangles*: hH1B ($n = 9$); *squares*: hH1AB ($n = 7$). Lines represent point-to-point curves of the chimera data "shifted" by 7–10 mV in the depolarized direction along the voltage axis. The magnitude of the imposed shift was determined by the shift in V_a measured in Fig. 2. *Long dash*: hH1A shifted 7.4 mV; *dots*: hH1B shifted 6.8 mV; *dash-dot-dot*: hH1AB shifted 10.1 mV.

plasmic loops activate only following greater depolarizations, while lesser depolarizations are required to activate channels containing one or both of the skeletal muscle channel cytoplasmic loops. Note also that the slopes of the *G-V* relationships for the chimeras are not significantly different from the wild-type slopes. The average activation voltages and slope factors, as well as the average values ± SEM for each gating parameter discussed here are listed in Table 1.

Loop-Dependent Shifts in Inactivation Time Constants Are Consistent in Direction and Magnitude with the Measured Shifts in Channel Activation Voltage

Figure 3*A* plots the measured time constants of inactivation (τ_h) as a function of membrane potential for hSkM1 versus its three chimeras. Note that inactivation times are shifted to the right for all three chimeras, with hSKM1AB shifted more than either single-loop chimera.

Figure 3*B* shows τ_h as a function of membrane potential for hH1 versus its three chimeras. Note here that the three chimeras are shifted to the left, with hH1AB shifted more than either single-loop chimera.

The curves shown in both figure panels reflect a shift of chimera data along the voltage axis of the same magnitude as the shifts in chimera V_a measured in Fig. 2 (compared to wild-type V_a). Note that for all six chimeras, this imposed linear shift along the voltage axis produces curves that nearly overlay wild-type data, indicating that the measured differences in τ_h with changing cytoplasmic loops mimic the shifts in channel activation voltage measured. As described in the Discussion section, it is likely that measured shifts in τ_h are due to a redistribution of channels between the closed and open states, resulting from the direct and isoform-specific effect of DI-II and/or DII-DIII linkers on channel activation voltage. That is, as shown in Fig. 2 above, the linker species directly alters activation voltage. This will change the percentage of channels in the open state at a single membrane potential. The percentage of open channels will directly affect the rate of transition from active to inactive channels through the process of mass action, and thus a change in τ_h may be measured with no direct effect on the inactivation process. This suggested indirect effect on the rate of channel inactivation is corroborated by the data shown in Figs 4–6 that show no direct isoform-specific loop effect on other gating parameters.

Steady-State Inactivation Is Unaffected by Swapping Cytoplasmic Loops

To determine more directly whether the species of cytoplasmic loop(s) affects the distribution of channels between states other than the closed to open distribution (as indicated by shifts in V_a), steady-state inactivation curves were measured for each construct. Figures 4*A* and 4*B* reflect the fraction of channels that remain available for activation following a 500 ms prepulse depolarization of varying magnitude. Note that while hSkM1 and hH1 have different half-inactivation voltages (V_i; ~ -56 and ~ -65 mV for hSkM1 and hH1, respectively-*see* Table 1), the replacement of one isoform's cytoplasmic loops with loops from the other isoform has no sig-

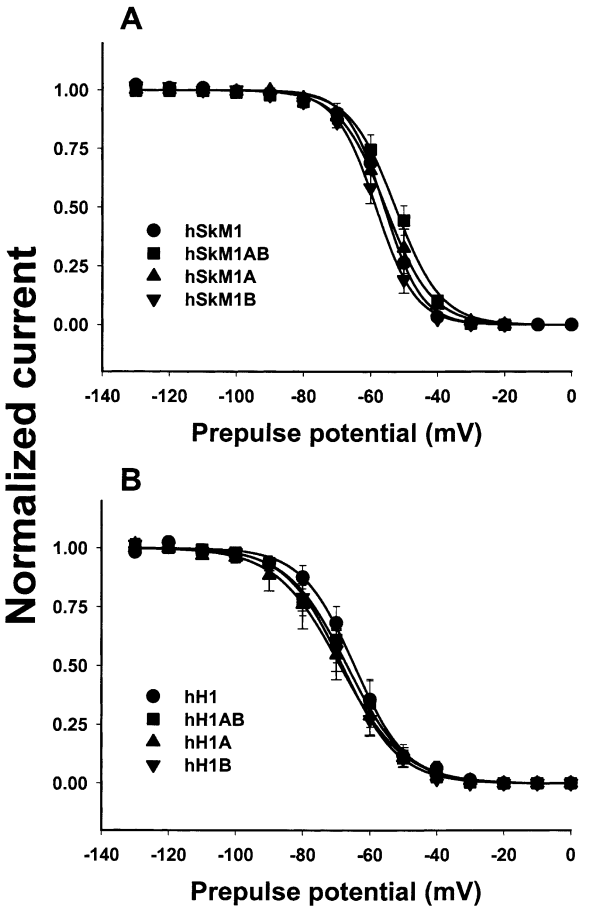

Fig. 4. The species of cytoplasmic loop does not affect steady state inactivation. Steady-state inactivation (h_{inf}). Data are the average normalized current ± SEM measured during a 5 ms pulse to +60 mV following a 500 ms prepulse to the plotted potentials. Curves are fits of the data to single Boltzmann distributions. (*A*) h_{inf} for hSkM1, hSkM1A, hSkM1B, and hSkM1AB. *Circles*: hSkM1; *triangles*: hSkM1A; *inverted triangles*: hSkM1B, *squares*: hSkM1AB. $n = 9$ for each set of data. (*B*) h_{inf} for hH1, hH1A, hH1B, and hH1AB. *Circles*: hHl ($n = 13$); *triangles*: hH1A ($n = 8$); *inverted triangles*: hH1B ($n = 9$); *squares*: hH1AB ($n = 7$).

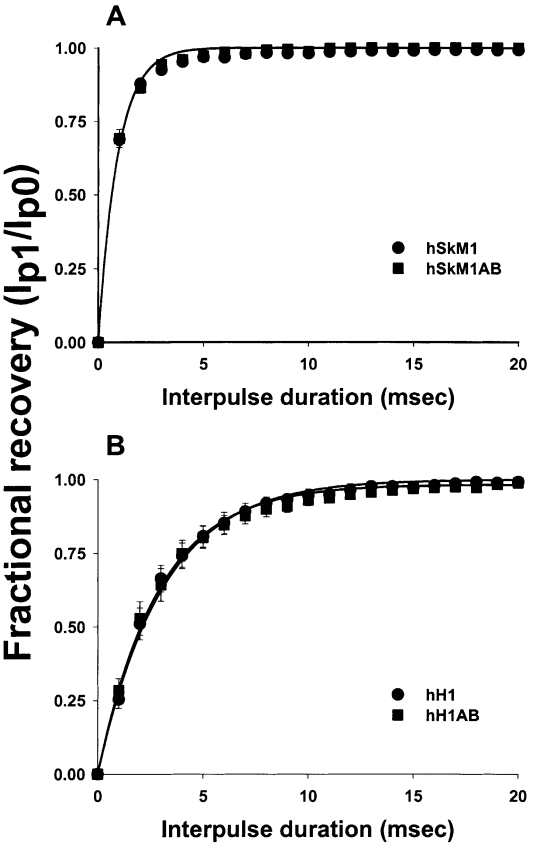

Fig. 5. Swapping cytoplasmic loop does not alter the time to recovery from inactivation at −120 mV. Recovery from inactivation at a −120 mV recovery potential. Data represent the average fractional current ± SEM measured following a −120 mV recovery potential of varied duration, ranging from 1 to 20 msec. Curves are fits of the data to single exponential functions. (*A*) Fractional current as a function of recovery time for hSkM1, hSkM1A, hSkM1B, and hSkM1AB. *Circles*: hSkM1; *triangles*: hSkM1A; *inverted triangles*: hSkM1B; *squares*: hSkM1AB. n = 9 for each set of data. (*B*) Fractional current as a function of recovery time for hH1, hH1A, hH1B, and hH1AB. *Circles*: hH1 ($n = 13$); *triangles*: hH1A ($n = 8$); *inverted triangles*: hH1B ($n = 9$); squares: hH1AB ($n = 7$).

nificant effect on the availability curves. These data indicate that the distribution of channels into the inactivated state is not affected differently by the various species of cytoplasmic loop(s) studied here.

The Rate and Voltage Dependence of Recovery from Fast Inactivation Are not Altered by Changing Cytoplasmic Loops

To test the possibility that the distribution of channels back into the closed state from the inactivated state (i.e., recovery from fast inactivation) is dependent directly on the species of cytoplasmic loop(s) attached to the channel, the rate of recovery from inactivation was measured for hSkM1, hH1, and both double-loop chimeras. Figures 5*A* and 5*B* show the fractional current measured during the second test pulse of a twin pulse protocol, in which the second pulse follows the first test pulse by increasing times ranging from 1 to 20 ms, holding the potential at a −120 mV between pulses. Note that while the time constants for recovery from inactivation (τ_{rec}) for hSkM1 constructs are significantly faster than τ_{rec} for hH1 constructs (~0.9 and ~2.9 ms for hSkM1 and hH1, respectively), the double-loop chimeras show τ_{rec} nearly identical to their wild-type counterparts at the −120 mV recovery potential.

The τ_{rec} as a function of recovery potential were then measured for hSkM1, hH1, and the two double-loop chimeras, as shown in Fig. 6. The data show that while hSkM1 and hH1 have distinct recovery profiles, τ_{rec} as a function of recovery potential for each double-loop chimera mimics the τ_{rec} of its wild-type

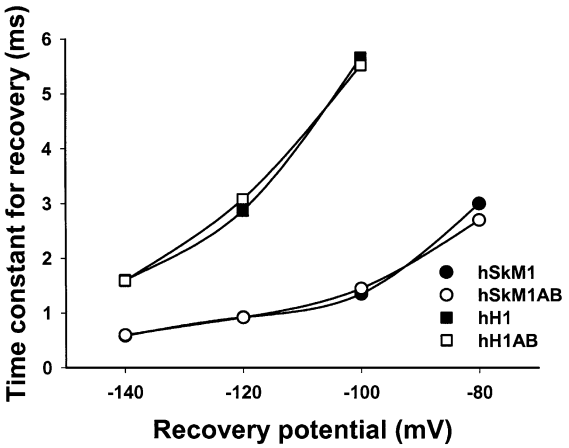

Fig. 6. The potential dependence of τ_{rec} is not dependent on the species of cytoplasmic loops. Data are τ_{rec} measured at the plotted recovery potentials, determined by fitting data similar to that shown in Fig. 5 to single-exponential functions, as described in the Methods section. Curves are non-theoretical, point-to-point. *Filled Circles*: hSkM1 ($n = 9$); *empty circles*: hSkM1AB ($n = 9$); *filled squares*: hH1 ($n = 13$); *empty squares*: hH1AB ($n = 7$).

counterpart. Thus, the cytoplasmic loops A and B do not seem to impose any direct, isoform-specific effect on the recovery from inactivation, either in rate of recovery or in its potential dependence.

The Cytoplasmic Loops Contribute Directly to the Size of the Window Current

The combined distribution of channels between the open and inactivated states at a membrane potential affects the percentage of channels that are persistently active. This distribution can be represented graphically by overlapping *G-V* and steady-state inactivation curves as shown in Fig. 7, and is referred to as the "window current" (Attwell et al., 1979). Figure 7*A* plots the *G-V* and h_{inf} curves for hSkM1 and its chimeras (*top panel*), while the bottom panel shows the steady-state curves for hH1 and its chimeras. Note that a difference in window current among channel constructs is predicted, albeit difficult to assess quantitatively. Thus, Fig. 7*B* shows magnified versions of these *G-V* and h_{inf} curves. The bell-shaped curves on these figures are the product of the *G-V* and h_{inf} Boltzmann distributions (product of Eqs. 1 and 2) and they represent predicted persistent channel activity (conductance) (*see* Rugiero et al., 2003 for details). Note that constructs containing one or both of the hSkM1 linker loops have markedly larger predicted persistent activation. The predicted peak persistent activation is represented graphically in Fig. 7*C*. Constructs that contain both hSkM1 loops (hSkM1 and hH1AB) are predicted to have more than three times the peak persistent activity than those that contain both hH1 loops, with absolute values ranging from 0.4% (hH1, hSkM1AB) to 1.2% (hSkM1, hH1AB) of the peak conductance. Data corroborate these predictions. At small depolarizations, constructs containing the hSkM1 cytoplasmic loops maintained 2–3 times more residual current at the end of a 10 ms test depolarization than did the constructs containing hH1 loops (*data not shown*). These data indicate that the species of cytoplasmic linker attached to a channel alters the window current for that construct, and thus directly affects the percentage of persistently active channels, which may have a significant impact on resting membrane potential and the overall excitability of the cell.

Changes in Internal Ionic Strength Verify that Loop-specific Contributions to an Internal Surface Potential Can not Account for Loop-specific Effects on V_a

The data shown above indicate that only channel activation voltage is differently impacted by the species of cytoplasmic loop(s) A and/or B that is attached to the channel, such that channels containing skeletal muscle channel loops A and/or B activate at more hyperpolarized potentials than channels that contain cardiac channel loops A and/or B. There is a possibility that the isoform-specific changes in channel activation voltage are caused by differences among these cytoplasmic loops in their contribution to an internal surface potential.

It is established that channel activation voltage is partially dependent on a certain set of internal (as well as external) charges aligned near the membrane surface that impose some effect on the electric field sensed by the gating mechanism of the channel (Cukierman et al., 1988; Chabala et al., 1991; Cukierman, 1991; Cukierman and Krueger, 1991). The charged amino-acid residues within the hH1 and hSkM1 cytoplasmic loops may contribute to this internal surface potential, and differences among the loops in the number and location of charged amino acids that contribute to a surface charge would produce varying surface potentials. As such, we set out to test the hypothesis that the isoform-specific direct effect of the cytoplasmic loops on channel activation voltage is caused by loop-specific differences in internal surface potential.

The *G-V* relationships were determined for hSkM1, hH1, and each double-loop chimera under high and lower intracellular ionic strength. With the lowered ionic strength, screening of internal surface charges should be minimized, and the effect of any internal surface potential on channel activation voltage should be greater, measured as a shift in channel activation voltage. If there are differences in the surface potential produced by the different cytoplasmic loops, then the shifts in V_a with changing internal ionic strength should vary among the constructs. Figure 8 shows that for all four constructs, increasing ionic strength causes a similar 8–11 mV hyperpolar-

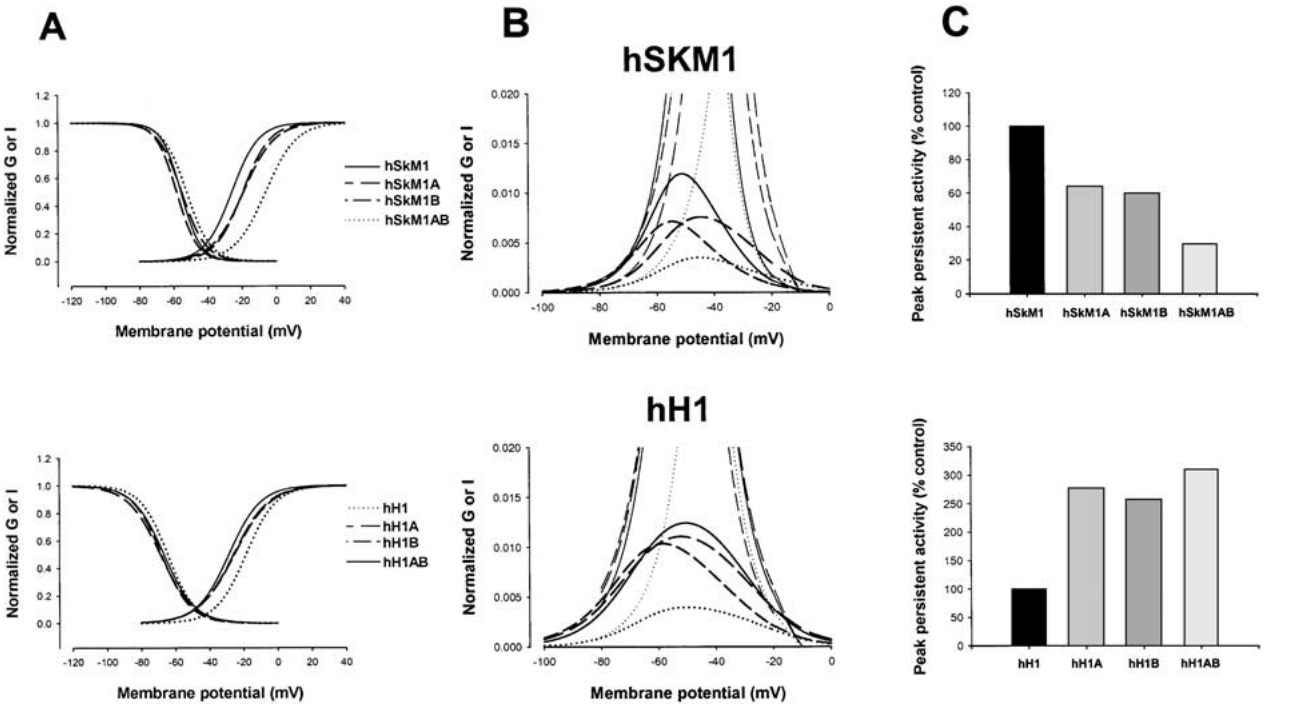

Fig. 7. The magnitude of the window current is dependent consistently on the species of cytoplasmic loop. *Panel A*: Boltzmann distributions of steady-state activation (*G-V*) and inactivation curves (h_{inf}) for all tested constructs. *Top*: hSkM1 (*solid line*), hSkM1A (*long dash*), hSkM1B (*medium dash*), and hSkM1AB (*dots*). *Bottom*: hH1 (*dots*), hH1A (*long dash*), hH1B (*medium dash*), and hH1AB (*solid line*). *Panel B*: Persistent channel activity. Upper curves in each panel are the *G-V* and h_{inf} curves for all tested constructs. Bell-shaped curves represent the product of the activation and inactivation Boltzmann distributions, and indicate the persistent channel activity (Rugiero et al., 2003). *Top*: hSkM1 (*solid line*), hSkM1A (*long dash*), hSkM1B (*medium dash*), and hSkM1AB (*dots*). *Bottom*: hH1 (*dots*), hH1A (*long dash*), hH1B (*medium dash*), and hH1AB (*solid line*). *Panel C*: Peak persistent activity. Bars represent the peak persistent activity calculated from the bell-shaped curves shown in Panel *B* and normalized to wild-type peak persistent activity (hSkM1: *top*; hH1: *bottom*). *Top*: hSkM1, hSkM1A, hSkM1B, and hSkM1AB. Bottom: hH1, hH1A, hH1B, and hH1AB.

izing shift in channel V_a. Given the very similar shifts in V_a with changing ionic strength among the constructs, one can conclude that differences in surface potential produced by the different cytoplasmic loops can not account for the much larger (nearly 20 mV), direct, isoform-specific effects of these loops on channel activation voltage.

Discussion

Only Activation Voltage is Directly Altered in an Isoform-Specific Manner by the Structurally Divergent DI-DII and DII-DIII Linkers

Figures 2–6 illustrate that the species of cytoplasmic loop(s) A and/or B attached to either the cardiac or skeletal muscle sodium channel directly affects only channel activation voltage. As shown in Fig. 2, channels containing cardiac channel loop(s) A and/or B activate at potentials more positive than do channels containing skeletal muscle channel loop(s) A and/or B. Interestingly, as shown in Fig. 2 and quantified in Table 1, there is no significant difference in the Boltzmann slope factor (K_a) with changing cytoplasmic loop. Thus, the data consistently indicate some direct, isoform-specific effect of these cytoplasmic loops on channel activation voltage that produces a linear shift along the voltage axis. Given this shift along the voltage-axis, it is not unreasonable to expect isoform-specific effects on other voltage-dependent gating parameters.

Of the other gating parameters measured, only the rate at which a channel inactivates showed any significant dependence on the species of cytoplasmic loop(s) (*see* Fig. 3). However, the measured loop-specific shifts in τ_h appear to be indirect, likely caused by the kinetic coupling between active and inactive channel states. Such an indirect effect is indicated for several reasons: 1) The effect of changing loops on inactivation rates is nearly identical, both in direction and in voltage dependence, to the effect of these loops on channel activation voltage (*compare* Figs. 2 and 3). 2) The loop species has no isoform-specific effect on steady-state inactivation (channel availability, *see* Fig. 4). 3) The loop species has no isoform-specific effect on the time or voltage dependence of recovery

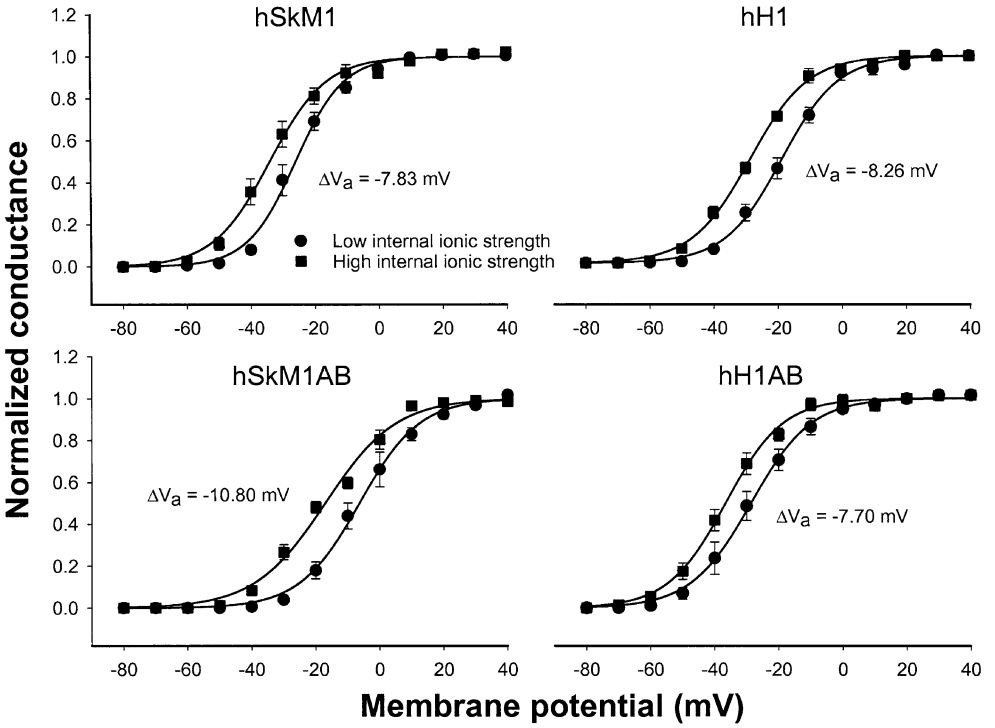

Fig. 8. Isoform-specific effects of cytoplasmic loops on channel activation voltage can not be explained through an electrostatic mechanism. *G-V* relationships for hSkM1, hSkM1AB, hH1, and hH1AB measured under conditions of lower (*filled circles*: number of samples as listed in Fig. 2) and high (*filled squares*: $n = 7$ for all constructs) internal ionic strength. Internal and external Na^+ concentrations were constant. Lower ionic strength is as listed in the Methods section. For the higher ionic strength solution, 60 mM CsCl replaced 120 mM sucrose. Data are the mean ± SEM conductance at a membrane potential. Curves are fits of the data to single Boltzmann distributions.

from inactivation (Figs. 5 and 6). 4) There is no indication that the loop species differently affects other gating parameters such as closed-state inactivation. The data shown in the availability curves of Fig. 4 are consistent with all channels being fully available for activation at the −100 mV holding potential.

Thus, the data indicate that there is not a direct, isoform-specific effect of cytoplasmic loops on inactivation rates. Rather, this measured shift in channel inactivation rate with changing loop(s) can be explained by a redistribution of channels into or from the open state. The transition rate from the open to the inactivated state is kinetically coupled to other channel state transitions. When the density of channels in the open state is altered, the measured rate of transition from the open to the inactivated state will be affected similarly. The data shown in Fig. 2 indicate that the cytoplasmic loop species attached to the channel directly affects channel V_a. Channel V_a reflects the distribution of channels in the open state as a function of membrane potential. Because V_a shifts depending on the identity of the cytoplasmic loop(s), the percentage (density) of channels in the open state at a given membrane potential is loop-dependent. Thus, the rate of transition into the inactivated state from the open state subsequently will be altered similarly. This is illustrated by the curves drawn in Fig. 3, which represent a shift in τ_h that is very similar to the shift in V_a measured in Fig. 2, indicating that there is no direct, isoform-specific effect of these cytoplasmic loops on τ_h.

Together, the data shown in Figs. 2–6 suggest that only channel activation voltage is directly altered by the cytoplasmic loop(s) A and/or B that is attached to the channel. This is quite novel. Nearly all previous data assign roles for the cytoplasmic portions of the channel in inactivation mechanisms, both fast and slow, as well as effects on surface expression, generally caused by posttranslational modifications made to these cytoplasmic structures (*see*, for e.g., Wieland et al., 1996; Frohnwieser et al, 1997; Smith and Goldin, 2000; Alekov et al., 2001; Wan et al., 2001; Deschenes et al., 2002). This report serves to indicate yet an additional effect of the cytoplasmic channel structures on channel function: specific, differential, and direct effects of the cytoplasmic loops on channel activation voltage.

The Magnitude of the Window Current is Loop-specific—This will Likely Impact the Resting Membrane Potential of the Cell and its Overall Excitability

Further, the data indicate that the effect of cytoplasmic loops on channel V_a is isoform-specific, with

cardiac channel loops shifting activation voltage in the depolarized direction, and skeletal muscle channel loops shifting activation voltage in the hyperpolarized direction. The relevance of this finding is significant. It indicates that although these loop structures among isoforms are not well conserved, only one gating parameter, channel activation voltage, is altered directly and differently by these divergent loop structures. Physiologically, this may have a major impact on the overall excitability of the cell. As shown in Fig. 7, the window current, which indicates the level and voltage-distribution of persistently active channels, is directly altered by which linker species (loops A and/or B) is/are attached to a channel. That is, the data suggest that channels containing skeletal muscle channel linkers have more than three times the peak persistent activation than do constructs that contain cardiac channel linkers. This apparent three-fold increase in persistent activity may affect the ability of the cell to fire action potentials. There are several reports which indicate that point mutations of SCN1A and SCN5A localized to putatively cytoplasmic regions of the channels cause small increases in the magnitude of the window current that produce tiny increases in persistent sodium current (on the order of a 1% increase, similar to the isoform-specific difference in peak persistent activity observed here). This persistent sodium current may be solely responsible for such maladies as epilepsy and arrhythmias (LQTS) (Wang et al., 1996; Abriel et al., 2001; Lossin et al., 2002; Splawski et al., 2002; Spampanato et al., 2003). These reports indicate the vital need for a delicate balance between the voltage dependencies of sodium channel activation and inactivation, and the rather significant impact of slight changes to this balance on the excitability of the affected tissue. Here, the data indicate that the structurally divergent DI-DII and DII-DIII linkers alter only the window current in an isoform-specific manner. This suggests a rather elaborate and novel mechanism by which isoform-specific sodium channel activation voltages, and thus window currents, are created and thereby impact the ability of the cell to fire an action potential.

What are the Possible Mechanisms, and Are they Plausible?

There must be structural differences among the loops of these two channel isoforms that directly and differently alter only channel activation voltage, and thus impact the overall excitability of the cell by changing the size of the window current. But, what are these structural differences, and by what mechanism do they impose this loop-specific effect only on channel activation voltage?

We begin this analysis by discussing three possible mechanisms: 1) an electrostatic mechanism, in which the isoform-specific loops contribute differently to an internal surface potential, 2) differential phosphorylation, and 3) isoform-specific interactions of the cytoplasmic loops with the cytoskeleton or some other yet to be determined cytoplasmic protein (or the channel itself) that leads to isoform-specific differences in channel activation voltage. Any or all of these mechanisms are possible. We have described a phenomenon in which two different cytoplasmic loops from a single isoform (loops A and B) have seemingly similar effects on channel activation voltage. However, there is no reason a priori that the mechanisms by which both cytoplasmic loops alter channel activation voltage must be identical. What follows is a description of each of these possible mechanisms and of the data gathered here and in previous work that allows one to exclude possible mechanisms.

An Electrostatic Mechanism Can not Account for the Isoform-specific Effect of Cytoplasmic Loops on Activation Voltage

It is possible that the loop- and isoform-specific effects on channel V_a observed here is caused by differential contributions of the various cytoplasmic loops to an internal surface potential. Each loop may contribute charges to an overall surface potential that alters the electric field sensed by the channel gating mechanism. If the contribution to this surface potential is loop-specific, then the activation voltage would be somewhat dependent on the species of loop attached to the channel (i.e., an electrostatic mechanism).

Previous studies indicated the presence of an internal surface potential that alters channel activation voltage (Cukierman et al., 1988; Chabala et al., 1991; Cukierman, 1991; Cukierman & Krueger, 1991). One can screen effectively the contribution of these charges to a surface potential by using increasing internal divalent ion concentrations or ionic strength, typically producing a measured hyperpolarizing shift in channel activation voltage.

Here, we sought to question directly whether differences in internal surface potential between cardiac and skeletal muscle channel cytoplasmic loops might be responsible for the different activation voltages measured in Fig. 2. Because the data shown in Figs. 4–6 do not show similar shifts in other voltage-dependent parameters, one might rule out such an electrostatic mechanism, especially since previous studies of external surface potential on sodium channel function showed similar shifts in all voltage-dependent parameters with changes in external surface potential (Hahin and Campbell, 1983; Bennett et al., 1997; Bennett, 2002). However, the lack of a consistent shift in all voltage-dependent parameters is not adequate to rule out the possibility that the

electric field sensed by a particular gating mechanism is altered by changes in surface potential. In fact, others have concluded that non-uniform shifts in voltage-dependent gating parameters might be explained through an electrostatic mechanism (Frankenhauser and Hodgkin, 1957; Zhang et al, 1999; Tyrrell et al., 2001). Thus, direct measurement of the effects of changing internal surface potential among constructs should indicate whether the different loops impose functionally relevant changes in internal surface potential. As shown in Fig. 8, increasing the internal ionic strength produces a hyperpolarizing shift in the V_a for all constructs, indicating a screening of an internal negative surface potential with increasing internal ionic strength.

If there is a functionally relevant difference among the cytoplasmic loops in the relative contribution each makes to this internal surface potential, then one would predict that the changes in internal ionic strength would show isoform-specific shifts in channel V_a. As shown in Fig. 8, the V_a for each construct shifts in the hyperpolarized direction by 8–11 mV following the increase in internal ionic strength. This indicates that there is no significant difference among the constructs in their contribution to an internal surface potential, and thus, an electrostatic mechanism can not account for the much larger differences in V_a (up to nearly 20 mV) observed among specific cytoplasmic loops.

It Is Unlikely that Isoform-specific Differential Phosphorylation of the Cytoplasmic Loops Can Account for the Measured Changes in Channel Activation Voltage

While the full extent of phosphorylation of hSkM1 and hH1 is not yet known, most data indicate that the loop joining domain I to II (loop A) tends to be heavily, and differently (between hSkM1 and hH1) phosphorylated, while loop B, joining domain II to III is only slightly, or not at all phosphorylated (for reviews, *see* Catterall, 1997; Rossie, 1999; Schreibmayer, 1999). This difference between loop A and loop B in levels of phosphorylation in concert with the data presented here, which indicate nearly equivalent contributions by each loop on V_a, suggests that differences in phosphorylation between hH1 and hSkM1 may not explain the isoform-specific effects on channel activation voltage observed here.

Many studies have questioned the isoform-specific role of phosphorylation in sodium channel function, looking at the direct effects of protein kinase A (PKA) and protein kinase C (PKC) phosphorylation as well as the indirect effects of G protein and cAMP activation on channel function in addition to other kinase or phosphatase activity (Sorbera & Morad, 1991; Matsuda et al., 1992; Bendahhou et al., 1995; Catterall, 1997; Chahine & George, 1997; Frohnwieser et al., 1997; Desaphy, DeLuca & Camerino, 1998; Lu et al., 1999; Rossie, 1999; Schreibmayer, 1999; Patel et al., 2000; Ratcliffe et al., 2000; Deschenes et al., 2002). Most reports show an increase or decrease in peak sodium current, consistent with an increase or decrease in channel surface density. Some reports indicate a slight change in channel inactivation, either in the kinetics, or steady state, or both. However, all data indicate that such phosphorylation has no effect on the voltage dependence of channel activation. Directly to the point at hand, one report compared the effects of PKA phosphorylation of rat $Na_{v1.4}$ and human $Na_{v1.5}$ as well as several chimeras of the two isoforms in which permutations of channel domain combinations were assembled into novel channel constructs. The activation voltages among these constructs were unaffected by phosphorylation (Frohnwieser et al., 1997). While one can not explicitly rule out the possibility that some novel kinase may cause differential phosphorylation of sodium channel cytoplasmic loops that is responsible for the measured shifts in V_a, studies of kinase effects on sodium channel function to date all indicate that it is unlikely that these differences in phosphorylation can account for the measured shifts in channel V_a.

Might Isoform-specific Interactions with Cytoplasmic Proteins Account for the Loop-dependent Shifts in Channel Activation Voltage?

Another possible mechanism by which isoform-specific loops might impose differing effects on channel activation voltage could be through differential interaction of the loops with the cytoskeleton or other proteins. For example, if the cardiac channel loops interact with the cytoskeleton such that the activation gating mechanism lies at some point in the electric field, then the channel will activate following a given depolarization due in part to this interaction with the cytoskeleton. If this interaction is altered, perhaps broken through papain treatment, or altered through interaction of the cytoskeleton with a different cytoplasmic loop, then the impact of this interaction on the channel gating mechanism might be either absent or altered, setting the gating mechanism to a different position within the electric field, thus causing the channel to activate at a different depolarization.

This scenario might explain the isoform-specific differences in function imposed by the cardiac versus skeletal muscle channel loops. However, the data gathered to question the role of the cytoskeleton on sodium channel function, while limited, indicate that this is unlikely. Reports using cytochalasin D to disrupt F-actin polymerization indicate that there is no significant effect on cardiac or skeletal muscle sodium channel activation voltage (Undrovinas,

Shander & Makielski, 1995; Maltsev & Undrovinas, 1997; Moran et al, 2000). Only when a microtubule stabilizer, taxol, is used, did one study report a hyperpolarizing shift in cardiac channel activation voltage (Maltsev & Undrovinas, 1997). This shift was small, and, in fact, in the opposite direction as one would predict, assuming that differential interaction with the cytoskeleton is the mechanism responsible for the measured shift in channel activation voltage reported here.

While previous data indicate that typical cytoskeletal elements are not responsible for these loop-dependent activation voltages, detailed studies of more cytoskeletal elements in this system are needed to confirm or rule out a cytoskeleton-sodium channel loop interaction that directly alters channel V_a. In addition to differential interactions of the loops with cytoskeletal elements, it is intriguing to suggest that these loops may interact with some other protein (or perhaps the channel protein itself). The exact species of putative proteins with which these loops may interact is not yet known, but is the focus of future studies. Much remains to be done in order to determine the exact mechanism and structures responsible for this novel phenomenon, in which certain structurally divergent sodium channel cytoplasmic loops directly alter only channel activation voltage in an isoform-specific manner. This isoform-specific change in activation voltage leads to an apparent change in persistent channel activity that may directly affect the ability of the cell to fire action potentials.

This work was supported in part by grants from the American Heart Association, Florida Affiliate, and from the National Institute for Arthritis and Musculoskeletal and Skin Diseases.

References

Abriel, H., Candido, C., Wehrens, X.H.T., Rivolta, I., Motoike, H.K., Memmi, M., Napolitano, C., Prior, S.G., Kass R.S. 2001. Novel arrhythmogenic mechanism revealed by a Long-QT syndrome mutation in the cardiac Na^+ channel. *Circ. Res.* **88:**740–745

Alekov, A.K., Peter, W., Mitrovic, N., Lehmann-Horn, F., Lerche, H. 2001. Two mutations in the IV/S4-S5 segment of the human skeletal muscle Na^+ channel disrupt fast and enhance slow inactivation. *Neurosci. Lett.* **306:**173–176

Attwell, D., Cohen, I., Eisner, D., Ohba, M., Ojeda, C. 1979. The steady state TTX-sensitive ("window") sodium current in cardiac purkinje fibres. *Pfluegers Arch.* **379:**137–142

Bendahhou, S., Cummins, T.R., Potts, J.F., Tong, J., Agnew, W.S. 1995. Serine-1321-independent regulation of the mu 1 adult skeletal muscle Na^+ channel by protein kinase C. *Proc. Natl Acad. Sci. USA* **92:**12003–12007

Bennett, E., Urcan, M.S., Tinkle, S.S., Koszowski, A.G., Levinson, S.R. 1997. Contribution of sialic acid to the voltage dependence of sodium channel gating. A possible electrostatic mechanism. *J. Gen. Physiol.* **109:**327–343

Bennett, E.S. 1999. Effects of channel cytoplasmic regions on the activation mechanisms of cardiac versus skeletal muscle Na^+ channels. *Biophys. J.* **77:**2999–3009

Bennett, E.S. 2001. Channel cytoplasmic loops alter voltage-dependent sodium channel activation in an isoform-specific manner. *J. Physiol.* **535:**371–381

Bennett, E.S. 2002. Isoform-specific effects of sialic acid on voltage-dependent Na^+ channel gating: Functional sialic acids are localized to the S5-S6 loop of domain I. *J. Physiol.* **538:**675–690

Bennett, P.B., Yazawa, K., Makita, N., George, A.L., Jr. 1995. Molecular mechanism for an inherited cardiac arrhythmia. *Nature* **376:**683–685

Cannon, S.C., Brown, R.H., Jr., Corey D.P. 1991. A sodium channel defect in hyperkalemic periodic paralysis: potassium-induced failure of inactivation. *Neuron* **6:**619–626

Catterall, W.A. 1997. Modulation of sodium and calcium channels by protein phosphorylation and G proteins. *Adv. Sec. Mess. Phosphoprot. Res.* **31:**159–181

Chabala, L.D., Urban, B.W., Weiss, L.B., Green, W.N., Andersen, O.S. 1991. Steady-state gating of batrachotoxin-modified sodium channels. Variability and electrolyte-dependent modulation. *J. Gen. Physiol.* **98:**197–224

Chahine, M., George, A.L., Jr., Zhou, M., Ji, S., Sun, W., Barchi, R.L., Horn, R. 1994. Sodium channel mutations in paramyotonia congenita uncouple inactivation from activation. *Neuron* **12:**281–294

Chahine, M., George, A.L., Jr. 1997. Myotonic dystrophy kinase modulates skeletal muscle but not cardiac voltage-gated sodium channels. *FEBS Lett.* **412:**621–624

Cukierman, S. 1991. Asymmetric electrostatic effects on the gating of rat brain sodium channels in planar lipid membranes. *Biophys. J.* **60:**845–855

Cukierman, S., Krueger, B.K. 1991. Effects of internal divalent cations on the gating of rat brain Na + channels reconstituted in planar lipid bilayers. *Pfluegers Arch.* **419:**559–565

Cukierman, S., Zinkand, W.C., French, RJ., Krueger B.K. 1988. Effects of membrane surface charge and calcium on the gating of rat brain sodium channels in planar bilayers. *J. Gen. Physiol.* **92:**431–447

Cummins, T.R., Zhou, J., Sigworth, F.J., Ukomadu, C., Stephan, M., Ptacek, L.J., Agnew, W.S. 1993. Functional consequences of a Na^+ channel mutation causing hyperkalemic periodic paralysis. *Neuron* **10:**667–678

Desaphy, J.F., De Luca, A., Camerino, D.C. 1998. Blockade by cAMP of native sodium channels of adult rat skeletal muscle fibers. *Am. J. Physiol.* **275:**C1465–C1472

Deschenes, I., Neyroud, N., DiSilvestre, D., Marban, E., Yue, D.T., Tomaselli, G.F. 2002. Isoform-specific modulation of voltage-gated Na^+ channels by calmodulin. *Circ. Res.* **90:**E49–E57

Dumaine, R., Wang, Q., Keating, M.T., Hartmann, H.A., Schwartz, P.J., Brown, A.M., Kirsch, G.E. 1996. Multiple mechanisms of Na^+ channel-linked long-QT syndrome. *Circ. Res.* **78:**916–924

Fan, Z., George, A.L., Jr., Kyle, J.W., Makielski, J.C. 1996. Two human paramyotonia congenita mutations have opposite effects on lidocaine block of Na^+ channels expressed in a mammalian cell line. *J. Physiol.* **496:**275–286

Frankenhaeuser, B., Hodgkin, A.L. 1957. The action of calcium on the electrical properties of squid axon. *J. Physiol.* **137:**218–244

Frohnwieser, B., Chen, L.Q., Schreibmayer, W., Kallen, R.G. 1997. Modulation of the human cardiac sodium channel alpha-subunit by cAMP-dependent protein kinase and the responsible sequence domain. *J. Physiol.* **498:**309–318

Hahin, R., Campbell, D.T. 1983. Simple shifts in the voltage dependence of sodium channel gating caused by divalent cations. *J. Gen. Physiol.* **82:**785–802

Hayward, L.J., Brown, R.H., Jr., Cannon, S.C. 1996. Inactivation defects caused by myotonia-associated mutations in the sodium channel III-IV linker. *J. Gen. Physiol.* **107:**559–576

Ji, S., George, A.L., Jr., Horn, R., Barchi, R.L. 1996. Paramyotonia congenita mutations reveal different roles for segments S3 and S4 of domain D4 in hSkM1 sodium channel gating. *J. Gen. Physiol.* **107:**183–194

Lawrence, J.H., Orias, D.W., Balser, J.R., Nuss, H.B., Tomaselli, G.F., O'Rourke, B., Marban, E. 1996. Single-channel analysis of inactivation-defective rat skeletal muscle sodium channels containing the F1304Q mutation. *Biophys. J.* **71:**1285–1294

Lerche, H., Mitrovic, N., Dubowitz, V., Lehmann-Horn, F. 1996. Paramyotonia congenita: the R1448P Na^+ channel mutation in adult human skeletal muscle. *Ann. Neurol.* **39:**599–608

Lossin C., Wang, D.W., Rhodes, T.H., Vanoye, C.G., George, A.L., Jr. 2002. Molecular basis of an inherited epilepsy. *Neuron* **34:**877–884

Lu, T., Lee, H.C., Kabat, J.A., Shibata, E.F. 1999. Modulation of rat cardiac sodium channel by the stimulatory G protein alpha subunit. *J. Physiol.* **518:**371–384

Makita, N., Bennett, P.B., Jr., George, A.L., Jr. 1996. Multiple domains contribute to the distinct inactivation properties of human heart and skeletal muscle Na^+ channels. *Circ. Res.* **78:**244–252

Maltsev, V.A., Undrovinas, A.I. 1997. Cytoskeleton modulates coupling between availability and activation of cardiac sodium channel. *Am. J. Physiol.* **273:**H1832–H1840

Matsuda, J.J., Lee, H., Shibata, E.F. 1992. Enhancement of rabbit cardiac sodium channels by beta-adrenergic stimulation. Circ. Res. **70:**199–207

Moran, O., Tammaro, P., Nizzari, M., Conti, F. 2000. Functional properties of sodium channels do not depend on the cytoskeleton integrity. *Biochem. Biophys. Res. Commun.* **276:**204–209

Nagatomo, T., Fan, Z., Ye, B., Tonkovich, G.S., January, C.T., Kyle, J.W., Makielski, J.C. 1998. Temperature dependence of early and late currents in human cardiac wild-type and long Q-T DeltaKPQ Na^+ channels. *Am. J. Physiol.* **275:**H2016–H2024

Patel, M.K., Mistry, D., John, J.E., III., Mounsey, J.P. 2000. Sodium channel isoform-specific effects of halothane: protein kinase C co-expression and slow inactivation gating. *Br. J. Pharmacol.* **130:**1785–1792

Ptacek, L.J., George, A.L., Jr., Griggs, R.C., Tawil, R., Kallen, R.G., Barchi, R.L., Robertson, M., Leppert, M.F. 1991. Identification of a mutation in the gene causing hyperkalemic periodic paralysis. *Cell* **67:**1021–1027

Ptacek, L.J., George, A.L., Jr., Barchi, R.L., Griggs, R.C., Riggs, J.E., Robertson, M., Leppert, M.F. 1992. Mutations in an S4 segment of the adult skeletal muscle sodium channel cause paramyotonia congenita. *Neuron* **8:**891–897

Ratcliffe, C.F., Qu, Y., McCormick, K.A., Tibbs, V.C., Dixon, J.E., Scheuer, T., Catterall, W.A. 2000. A sodium channel signaling complex: modulation by associated receptor protein tyrosine phosphatase beta. *Nat. Neurosci.* **3:**437–444

Rossie, S. 1999. Regulation of voltage-sensitive sodium and calcium channels by phosphorylation. *Adv. Sec. Mess. Phosphoprot. Res.* **33:**23–48

Rugiero, F., Mistry, M., Sage, D., Black, J.A., Waxman, S.G., Crest, M., Clerc, N., Delmas, P., Gola, M. 2003. Selective expression of a persistent tetrodotoxin-resistant Na^+ current and $Na_V1.9$ subunit in myenteric sensory neurons. *J. Neurosci.* **23:**2715–2725

Schreibmayer, W. 1999. Isoform diversity and modulation of sodium channels by protein kinases. *Cell Physiol. Biochem.* **9:**187–200

Schwartz, P.J., Prior, S.G., Dumaine, R., Napoliano, C., Antzelevitch, C., Stramba-Badiale, M., Richard, T.A., Berti, M.R., Bloise, R. 2000. A molecular link between the sudden infant death syndrome and the Long-QT syndrome. *N. Engl. J. Med.* **343:**262–267

Smith, R.D., Goldin, A.L. 2000. Potentiation of rat brain sodium channel currents by PKA in *Xenopus* oocytes involves the I-II linker. *Am. J. Physiol.* **278:**C638–C645

Sorbera, L.A., Morad, M. 1991. Modulation of cardiac sodium channels by cAMP receptors on the myocyte surface. Science **253:**1286–1289

Spampanato, J., Escayg, A., Meisler, M.H., Goldin, A.L. 2003. Generalized epilepsy with febrile seizures plus type 2 mutation W1240R alters voltage-dependent gating of $Na_V1.1$ sodium channels. *Neurosci.* **116:**37–46

Splawski, I., Timoth, K.W., Tateyama, M., Clancy, C.E., Malhotra, A., Beggs, A.H., Cappuccio, F.P., Sagnella, G.A., Kass, R.S., Keating, M.T. 2002. Variant of SCN5A sodium channel implicated in risk of cardiac arrhythmia. *Science* **297:**1333–1336

Tyrrell, L., Renganathan, M., Dib-Hajj, S.D., Waxman, S.G. 2001. Glycosylation alters steady-state inactivation of sodium channel Nav1.9/NaN in dorsal root ganglion neurons and is developmentally regulated. *J. Neurosci.* **21:**9629–9637

Undrovinas, A.I., Shander, G.S., Makielski, J.C. 1995. Cytoskeleton modulates gating of voltage-dependent sodium channel in heart. *Am. J. Physiol.* **269:**H203–H214

Wan, X., Chen, S., Sadeghpour, A., Wang, Q., Kirsch, G.E. 2001. Accelerated inactivation in a mutant Na^+ channel associated with idiopathic ventricular fibrillation. *Am. J. Physiol.* **280:**H354–H360

Wang, D.W., Yazawa, K., George, A.L., Jr., Bennett, P.B. 1996. Characterization of human cardiac Na+ channel mutations in the congenital long QT syndrome. *Proc. Natl. Acad. Sci. USA* **93:**13200–13205

Wei, J., Wang, D.W., Alings, M., Fish, F., Wathen, M., Roden, D.M., George, A.L., Jr. 1999. Congential Long-QT syndrome caused by a novel mutation in a conserved acidic domain of the cardiac Na^+ channel. *Circulation* **99:**3165–3171

Wieland, S J., Gong, Q., Poblete, H., Fletcher, J.E., Chen, L.Q., Kallen, R.G. 1996. Modulation of human muscle sodium channels by intracellular fatty acids in dependent on the channel isoform. *J. Biol Chem.* **271:**19037–19041

Zhang, Y., Hartmann, H.A., Satin J. 1999. Glycosylation influences voltage-dependent gating of cardiac and skeletal muscle sodium channels. *J. Membrane Biol.* **171:**195–207